doi:10.1016/j.jmb.2004.04.051 *J. Mol. Biol.* (2004) **340**, 127–139

JMB

Available online at www.sciencedirect.com

SCIENCE DIRECT®

ELSEVIER

Rapid Self-assembly of α-Synuclein Observed by *In Situ* Atomic Force Microscopy

Wolfgang Hoyer[1], Dmitry Cherny[1,2], Vinod Subramaniam[3]* and Thomas M. Jovin[1]*

[1]*Department of Molecular Biology, Max Planck Institute for Biophysical Chemistry Am Fassberg 11, D-37077 Goettingen, Germany*

[2]*Institute of Molecular Genetics Russian Academy of Sciences Kurchatov's Square, 123182 Moscow, Russian Federation*

[3]*Biophysical Engineering Group, Faculty of Science and Technology, University of Twente, P.O. Box 217, 7500 AE Enschede, The Netherlands*

**Corresponding authors*

Self-assembly of α-synuclein resulting in protein aggregates of diverse morphology has been implicated in the pathogenesis of Parkinson's disease and other neurodegenerative disorders known as synucleinopathies. Apart from its biomedical relevance, this aggregation process is representative of the interconversion of an unfolded protein into nanostructures with typical amyloid features. We have used *in situ* tapping mode atomic force microscopy to continuously monitor the self-assembly of wild-type α-synuclein, its disease-related mutants A30P and A53T, and the C-terminally truncated variant α-synuclein(1–108). Different aggregation modes were observed depending on experimental conditions, i.e. pH, protein concentration, polyamine concentration, temperature and the supporting substrate. At pH 7.5, in the absence of the biogenic polyamines spermidine or spermine, elongated sheets 1.1(±0.2) nm in height and presumably representing individual β-sheet structures, were formed on mica substrates within a few minutes. Their orientation was directed by the crystalline substructure of the substrate. In contrast, sheet formation was not observed with hydrophobic highly oriented pyrolytic graphite substrates, suggesting that negatively charged surfaces promote α-synuclein self-assembly. In the presence of spermidine or spermine 5.9(±1.0) nm high spheroidal structures were preferentially formed, sharing characteristics with similar structures previously reported for several amyloidogenic proteins and linked to neurotoxicity. α-Synuclein spheroid formation depended critically on polyamine binding to the C terminus, revealing a promoting effect of the C terminus on α-synuclein assembly in the bound state. In rare cases, fibril growth from spheroids or preformed aggregates was observed. At pH 5.0, fibrils were formed initially and incorporated into amorphous aggregates in the course of the aggregation process, providing evidence for the potential of amyloid fibril surfaces to act as nucleation sites in amorphous aggregation. This study provides a direct insight into different modes of α-synuclein self-assembly and identifies key factors modulating the aggregation process.

Keywords: α-synuclein; atomic force microscopy; β-sheet; soluble oligomer; amyloid fibril

Introduction

The structural transition of the abundant protein α-synuclein from its monomeric form to aggregates rich in β-conformation has been implicated in the pathogenesis of Parkinson's disease (PD) and other neurological disorders.[1,2] Insoluble α-synuclein constitutes the main component of Lewy bodies and Lewy neurites, dense intra-neuronal inclusions of fibrillar and granular material that

Abbreviations used: Aβ, Alzheimer's β-amyloid peptide; AFM, atomic force microscopy; EPR, electron paramagnetic resonance; ESI-MS, electrospray ionization mass spectrometry; HOPG, highly oriented pyrolytic graphite; NMR, nuclear magnetic resonance; PD, Parkinson's disease; wt, wild-type; BCA, bicinchoninic acid.

E-mail addresses of the corresponding authors: v.subramaniam@tnw.utwente.nl; tjovin@gwdg.de

define PD neuropathologically.[1] Three missense mutations in the α-synuclein gene (A30P, A53T and E46K) have been linked to rare early-onset familial forms of PD, providing further evidence of the relevance of α-synuclein for PD.[3,4,60] Neuronal cell death seems to be a consequence of increased α-synuclein toxicity upon formation of aggregated structures, although the mechanism of toxicity remains unclear. Well-defined aggregation intermediates might account for much of the toxicity, a notion also suggested for other amyloidogenic proteins.[2,5–8]

α-Synuclein belongs to the group of natively unfolded proteins lacking ordered secondary structure *in vitro* in physiological buffers.[9] However, upon incubation at elevated temperatures with agitation, aggregates that share features typical of amyloid, e.g. fibrillar morphologies and high β-structure content, are formed and are reminiscent of the *in vivo* inclusions.[10–13] Electron paramagnetic resonance (EPR) and protease digestion studies concordantly report that the central 70–80 amino acid residues of the 140 amino acid protein constitute the aggregate core.[14,15] Whereas this region of the protein achieves a β-sheet conformation in the aggregated state, the C-terminal region comprising residues 103–140 remains unstructured.[14] This is probably a result of electrostatic repulsion within the C terminus as 14 out of the 37 C-terminal amino acid residues are acidic.

Although the C terminus is not incorporated into the aggregate core, it modulates the aggregation process. C-terminal truncated fragments aggregate faster than full-length α-synuclein, revealing that the C terminus hinders aggregation.[12,16,17] In addition, the C terminus can interact with cationic compounds such as metal ions by virtue of the accumulation of acidic residues, resulting in accelerated aggregation.[6,18–21] The polyamines putrescine, spermidine and spermine, naturally occurring polycations, are particularly effective in the promotion of α-synuclein assembly.[22] Their binding site has been localized to the C terminus (residues 109–140) by NMR.[23]

Other factors leading to an accelerated *in vitro* aggregation of α-synuclein are lower pH[21,24] and the disease-related A53T mutation.[12,25–28] Studies of the aggregation kinetics of the A30P mutant are inconclusive, with reports of faster aggregation,[26] similar aggregation speed,[12] or slower fibrillation but faster monomer consumption relative to the wild-type protein.[25,27,28]

Multimeric α-synuclein adopts a number of different morphologies, depending on aggregation incubation time and solution conditions. The earliest species detected by atomic force microscopy (AFM) demonstrate a bead-like structure with heights of 2–6 nm.[13,25,27,29] At later stages of the aggregation process, these globular structures are replaced by fibrillar species with distinctive morphologies. Apart from mature fibrils with heights of ~10 nm, smaller fibrils with heights of approximately 5 nm are formed, and have been proposed to be protofilaments.[13,25] In addition, annular species with diameters of 7–10 nm are found in early, pre-fibrillar fractions of α-synuclein incubations.[5,30] Under conditions linked to strong shielding of the negative charges in the C terminus, such as low pH or high metal ion or polyamine concentrations, α-synuclein aggregates exhibit an amorphous morphology, although the staining characteristics of amyloid are retained.[20–22]

The morphologies of different amyloidogenic peptides and proteins in the aggregated state show striking similarities, suggesting a common mode of assembly and potential toxicity.[31] Recent studies indicate that the early, pre-fibrillar aggregation intermediates possess the highest toxicity.[7,8] The *in vitro* toxicity of such soluble oligomers from different peptides and proteins is inhibited by a structure-specific antibody, implying a common, structure-based mechanism of toxicity.[8]

The complexity of the aggregation process arising from the structural polymorphism of the diverse intermediates and the dependence on solution conditions implies that direct and continuous observation of the reaction would be very desirable. *In situ* tapping mode AFM under liquid is a powerful tool for continuous observation of amyloid assembly.[32–34] The method enables the repeated imaging of mechanically delicate samples in physiological buffers and allows for selection of precisely defined solution conditions. In this study, we investigated the self-assembly of α-synuclein by *in situ* AFM.

Results

The following conditions were adopted for the

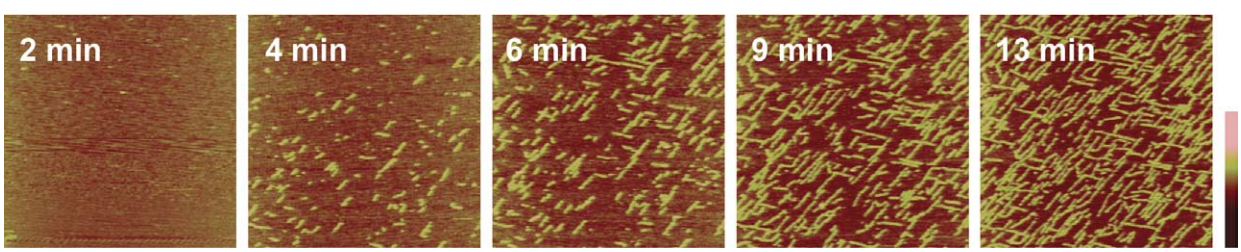

Figure 1. Surface-templated sheet formation by α-synuclein. Time series of 0.8 μm × 0.8 μm AFM height images. The experiment was performed at 33 °C in 25 mM Tris–HCl (pH 7.5), supplemented with 1 mM putrescine utilizing a mica substrate. At $t = 0$ monomeric α-synuclein was added to a final concentration of 8 μM. The height bar represents 5 nm.

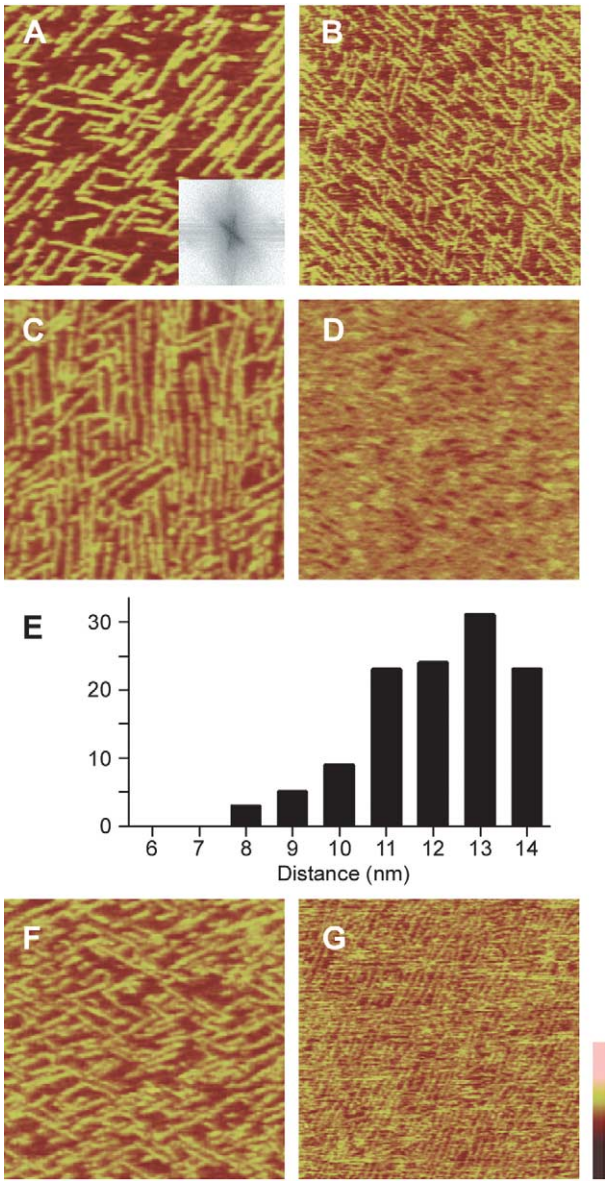

Figure 2. Condition-dependence of sheet formation. A, A 0.5 μm × 0.5 μm AFM height image; 33 °C; buffer, 25 mM Tris–HCl (pH 7.5), 1 mM putrescine; substrate, mica; protein concentration, 8 μM α-synuclein wt; *t*, 13 minutes. The height bar represents 5 nm. Inset, 2D Fourier transform of the image. B, A 0.64 μm × 0.64 μm AFM height image; 33 °C; buffer, 25 mM Tris–HCl (pH 7.5), no polyamine addition; substrate, mica; protein concentration, 40 μM α-synuclein wt; *t*, 24 minutes. The height bar represents 5 nm. C, A 0.35 μm × 0.35 μm AFM height image; 45 °C; buffer, 25 mM Tris–HCl (pH 7.5), 1 mM putrescine; substrate, mica; protein concentration, 40 μM α-synuclein wt; *t*, 25 minutes. The height bar represents 5 nm. D, A 0.35 μm × 0.35 μm AFM height image; 45 °C; buffer, 25 mM Tris–HCl (pH 7.5), 1 mM putrescine; substrate, mica; protein concentration, 40 μM α-syn(1–108); *t*, 16 minutes. The height bar represents 2.5 nm. E, Distribution of the lateral spacing of α-synuclein wild-type sheets, measured as the distance between the sheet axes. Only distances of <15 nm were considered; $n = 139$. F, A 0.5 μm × 0.5 μm AFM height image; 33 °C; buffer, 25 mM Tris–HCl (pH 7.5), 1 mM putrescine; substrate, mica; protein concentration, 40 μM α-synuclein A30P; *t*, 30 minutes. The height bar represents 3.5 nm. G, A 0.5 μm × 0.5 μm AFM height image; 33 °C; buffer, 25 mM Tris–HCl (pH 7.5), 1 mM putrescine; substrate, mica; protein concentration, 40 μM α-synuclein A53T; *t*, four minutes. The height bar represents 3.5 nm. Reported times indicate the time elapsed since monomer injection.

AFM studies. (i) The liquid cell was filled with the buffer (typically 25 mM Tris–HCl (pH 7.5)) and additives of choice and an initial image of the surface was acquired to confirm the absence of contaminating particles. (ii) Monomeric (according to analytical gel-filtration) α-synuclein was injected into the fluid cell and the assembly process monitored by continuous acquisition of AFM scans for ~45 minutes. (iii) The temperature was generally adjusted to either 33 °C or 45 °C by use of a custom tandem Peltier controller between the scanning head and the liquid cell. (iv) Measurements were generally performed at two different final protein concentrations (8 μM and 40 μM) in the absence and presence of one of the biogenic polyamines putrescine, spermidine or spermine at a final concentration of 1 mM.

In this study, we examined the full-length wild-type α-synuclein, the disease-related mutants with substitutions A53T and A30P, as well as a C-terminally truncated variant of the wild-type protein comprising amino acid residues 1–108 (syn(1–108)), thus lacking the polyamine-binding site. Two substrates of different chemical nature, freshly cleaved mica and highly oriented pyrolytic graphite (HOPG), were utilized to investigate the role of surface hydrophilicity/hydrophobicity in the aggregation process. Using this methodology, we were able to observe the formation of α-synuclein aggregates of different morphologies.

Assembly of 1.1 nm high, oriented sheets on hydrophilic mica

Figure 1 shows a time-course of wild-type α-synuclein self-assembly on a mica substrate in 25 mM Tris–HCl (pH 7.5) at a protein concentration of 8 μM in the presence of 1 mM putrescine at 33 °C. Under these conditions the surface became covered within a few minutes with elongated sheet-like structures with a height of 1.1(±0.2) nm ($n = 70$). The sheet lengths increased during the course of the experiment, indicating that the assembly proceeded as a surface phenomenon, as was also manifested by a preferential alignment along two specific directions. Two-dimensional Fourier transforms of height images from six different experiments (one of them shown in Figure 2A) revealed an angle of 120(±2)° between the two axes, presumably reflecting the pseudo-hexagonal geometry of the mica (001) surface.[35] Sheet formation was not observed when the hydrophilic mica substrate was replaced with the hydrophobic HOPG, giving further

support for a specific surface-dependent growth mechanism. Sheets were also formed in the absence of putrescine at a protein concentration of 40 μM (Figure 2B). However, at a protein concentration of 8 μM, sheets were formed in the presence of 1 mM putrescine (Figure 1), but not in the absence of the polyamine. Thus, both the protein and the putrescine concentration affected sheet formation. Experiments carried out at 45 °C did not reveal any temperature dependence of the aggregate morphology.

The individual sheets formed from wild-type α-synuclein were well resolved even in experiments in which the mica surface was saturated (Figure 2C). Analysis of the lateral spacing of sheets, measured as the distance between axes, yielded the distance distribution shown in Figure 2E (only distances <15 nm were considered). Lateral spacings below 10 nm were encountered only rarely and spacings of less than 8 nm were not observed. It is surprising that the individual sheets were generally well resolved, since object profiling by AFM is distorted due to convolution with the tip geometry (nominal tip radius 5–40 nm). In fact, deconvolution calculations led to an estimation of sheet width as <5 nm, i.e. the sheet width was distinctly smaller than the minimal lateral spacing between sheets. Consequently, the minimal lateral spacing must have originated from steric exclusion involving the object detected by AFM as well as additional unresolved structures.

The acidic C terminus of α-synuclein is not incorporated into the core of mature fibrils.[14,15,36] If the same situation was applied to the elongated sheets, the negatively charged C terminus might act as a spacer dictating the minimal separation due to charge repulsion. To test for such a possibility, *in situ* AFM experiments were performed with truncated α-synuclein syn(1–108) lacking the C terminus. Although sheet-like structures were formed by syn(1–108) (Figure 2D), they were less well resolved compared to those of wild-type α-synuclein. Parts of the mica surface appeared to be covered with diffuse layers of protein material instead of discrete sheets, implying a role of the C terminus in the regulation of the lateral spacing of full-length α-synuclein sheets.

Both disease-related mutants, A30P and A53T, formed sheet-like structures with heights of ~1 nm. Whereas self-assembly from A30P was indistinguishable from wild-type aggregates (Figure 2F), A53T aggregation occurred faster (full surface coverage was achieved in <1 minute) and resulted in less well organized sheets (Figure 2G). We conclude that the A53T mutant has a greater tendency for self-assembly than the wild-type and A30P mutant.

Rapid formation of 6 nm high spheroids under conditions linked to accelerated fibrillation

In the presence of 1 mM spermidine or spermine, formation of sheets was not observed. Instead, α-synuclein assembled primarily into 5.9(±1.0) nm ($n = 94$) high spherical or ellipsoidal particles with apparent widths of 15–20 nm (Figure 3). The dimensions of the individual spheroids did not change during the course of the experiment after their first appearance on the surface. Thus, their formation presumably occurs in solution independent of the substrate surface. *In situ* AFM experiments were carried out under various conditions to identify factors promoting/inhibiting spheroid formation.

Both the identity of the polyamine utilized (spermidine and spermine were required for spheroid assembly, putrescine was ineffective under the conditions employed) and its concentration affected the aggregation process. Figure 4 depicts aggregates formed at 45 °C from 8 μM protein solutions in the presence of 0.2 mM (A) and 1 mM (B) spermidine. In the presence of 0.2 mM spermidine the 1.1 nm high surface-aligned sheets were formed, whereas in 1 mM spermidine the protein assembled preferentially into the 6 nm high spheroids.

The protein concentration was an additional factor influencing spheroid formation. Figure 4C displays minor coverage of the mica surface with unordered protein at an α-synuclein concentration of 8 μM ($t = 33$ °C, 1 mM spermine). In contrast, at 40 μM protein and otherwise unchanged conditions, the formation of spheroids was extensive (Figure 4D).

Increased temperature was also associated with

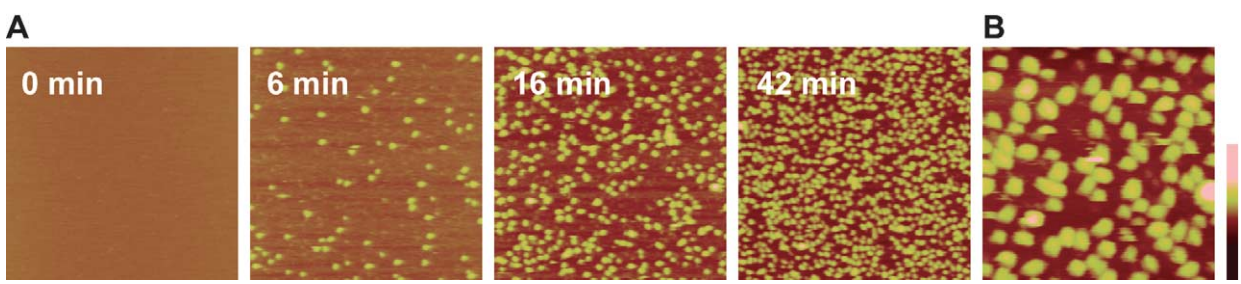

Figure 3. Spheroid formation by α-synuclein. A, Time series of 0.8 μm × 0.8 μm AFM height images. The experiment was performed at 33 °C in 25 mM Tris–HCl (pH 7.5), supplemented with 1 mM spermine utilizing a mica substrate. At $t = 0$ monomeric α-synuclein was added to a final concentration of 40 μM. The height bar represents 15 nm. B, The 0.25 μm × 0.25 μm AFM height image obtained from the same series 74 minutes after monomer injection.

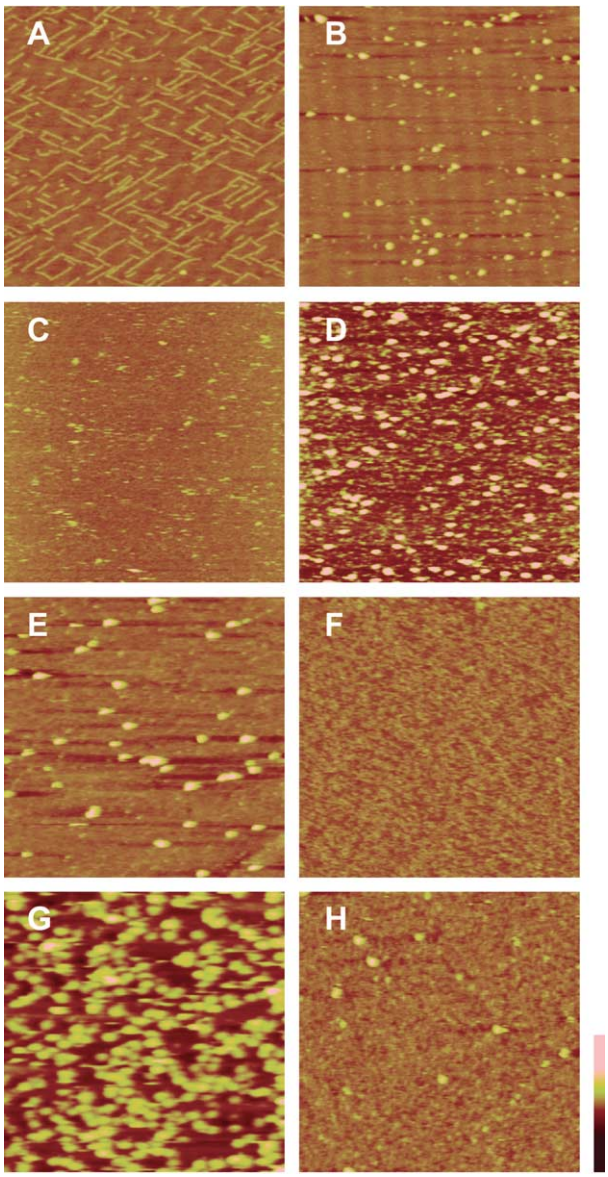

Figure 4. Condition-dependence of spheroid formation. The 1 μm × 1 μm AFM height images (except for G, 0.64 μm × 0.64 μm). A, At 45 °C; buffer, 25 mM Tris–HCl (pH 7.5), 0.2 mM spermidine; substrate, mica; protein concentration, 8 μM α-synuclein wt; *t*, 18 minutes. B, At 45 °C; buffer, 25 mM Tris–HCl (pH 7.5), 1 mM spermidine; substrate, mica; protein concentration, 8 μM α-synuclein wt; *t*, 17 minutes. C, At 33 °C; buffer, 25 mM Tris–HCl (pH 7.5), 1 mM spermine; substrate, mica; protein concentration, 8 μM α-synuclein wt; *t*, 15 minutes. D, At 33 °C; buffer, 25 mM Tris–HCl (pH 7.5), 1 mM spermine; substrate, mica; protein concentration, 40 μM α-synuclein wt; *t*, 19 minutes. E, At 33 °C; buffer, 25 mM Tris–HCl (pH 7.5), 1 mM spermine; substrate, HOPG; protein concentration, 40 μM α-synuclein wt; *t*, 14 minutes. F, At 33 °C; buffer, 25 mM Tris–HCl (pH 7.5), 1 mM spermine; substrate, mica; protein concentration, 40 μM α-syn(1–108); *t*, 14 minutes. G, At 33 °C; buffer, 25 mM Tris–HCl (pH 7.5), 1 mM spermine; substrate, mica; protein concentration, 40 μM α-synuclein A30P; *t*, 18 minutes. H, At 33 °C; buffer, 25 mM Tris–HCl (pH 7.5), 1 mM spermine; substrate, mica; protein concentration, 40 μM α-synuclein A53T; *t*, 28 minutes. The height bar represents 10 nm. Reported times indicate the time elapsed since monomer injection.

a stronger tendency for spheroid formation. These structures were not observed in experiments carried out at 33 °C with 8 μM protein and 1 mM spermidine or spermine (Figure 4C), but formed readily at 45 °C under otherwise identical conditions (Figure 4B).

In summary, spheroid formation was promoted by greater polyamine charge and concentration, protein concentration and temperature, factors known to accelerate α-synuclein fibrillation.[22,24,37] We conclude that the spheroids may function as important or essential on-pathway intermediates in fibrillation.

In contrast to the growth of 1.1 nm fibrils, spheroid formation was not impeded when the hydrophilic mica substrate was replaced with the hydrophobic HOPG (Figure 4E), supporting the notion that this process occurred in solution, i.e. not under the influence of the surface characteristics. In the case of the C-terminally truncated α-synuclein variant syn(1–108), spheroids did not form. Instead, a layer of precipitated material (height ~1 nm) without noticeable order appeared with 40 μM syn(1–108) in the presence of 1 mM spermine (Figure 4F). Thus, removal of the polyamine-binding site in the C terminus (residues 109–140) prevented spheroid formation.

Both disease-related mutants, A30P and A53T, formed spheroids with heights of ~6 nm under the conditions reported above for the wild-type protein. Spheroid formation of the A30P mutant was indistinguishable from wild-type aggregates (Figure 4G). However, fewer spheroids were observed with the A53T mutant compared to wild-type and A30P under identical conditions. Instead, the substrate was rapidly covered with a layer (height ~1 nm) of protein material without apparent organization (Figure 4H). This rapid surface precipitation was reminiscent of the situation in the absence of polyamines or in the presence of putrescine (Figure 2G), providing further evidence for a susceptibility of the A53T to precipitation on negatively charged surfaces.

Protofibril growth from spheroids

Scanning larger areas of the mica surface under conditions yielding spheroid aggregates revealed the presence of fibrillar structures with a height of ~6 nm as rare occurrences (Figure 5A and B). Although we cannot provide direct evidence for a relation of the ~6 nm high fibrils to mature α-synuclein fibrils with typical heights of ~10 nm, we denote the ~6 nm high structures as protofibrils in the following discussion in distinction to the ~10 nm mature fibrils. In general, the spheroids were stable as individual entities on the surface. For example, the coalescence of two or more individual spheroids was not observed. However, in rare cases protofibril growth from spheroids was observed (Figure 5C). Fibril elongation was bidirectional in the case shown in Figure 5C, but in other cases unidirectional. Heterogeneity in

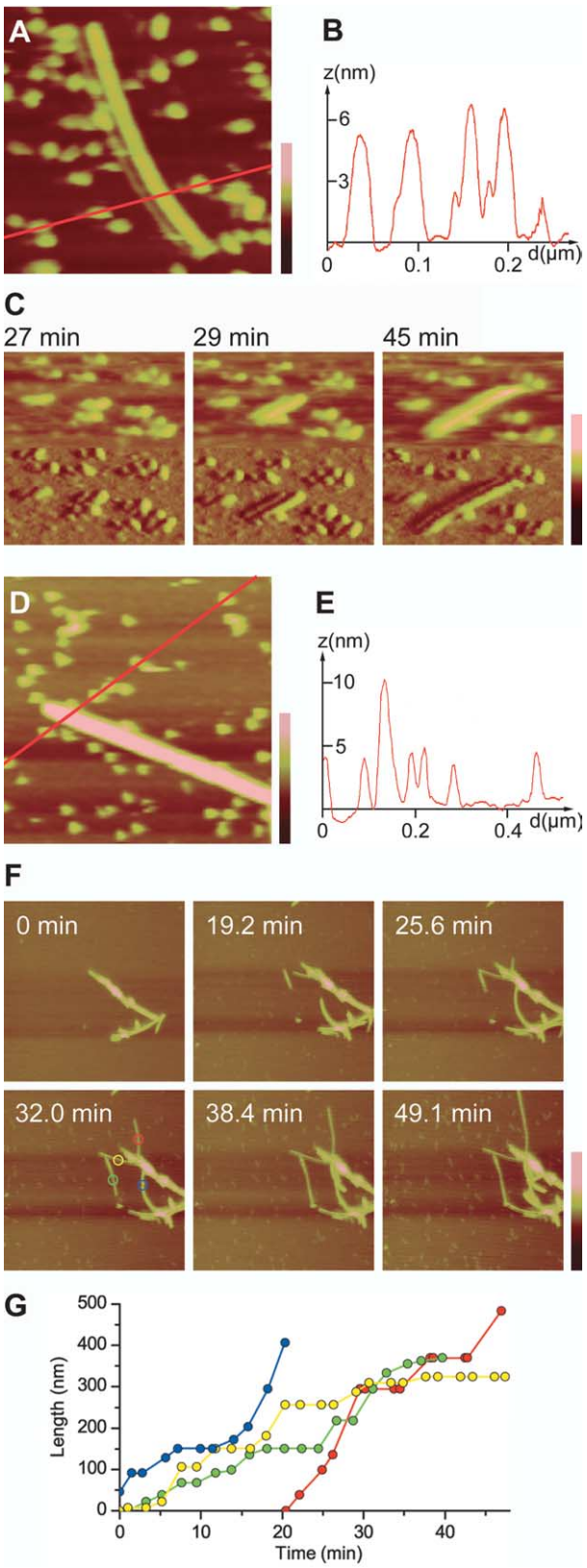

Figure 5. Protofibril growth observed by *in situ* AFM. A, The 0.25 μm × 0.25 μm AFM height image; 45 °C; buffer, 25 mM Tris–HCl (pH 7.5), 1 mM spermidine; substrate, mica; protein concentration, 40 μM α-synuclein wt; *t*, 47 minutes. The height bar represents 15 nm. B, Cross-section of image A. C, Time series of 0.31 μm × 0.17 μm AFM height (top half) and amplitude (bottom half) images. At 45 °C; buffer, 25 mM Tris–HCl (pH 7.5), 1 mM spermidine; substrate, mica; protein concentration, 40 μM α-synuclein wt. The height bar represents 15 nm. D, A 0.45 μm × 0.45 μm *ex situ* AFM height image; 100 μM α-synuclein wt was incubated at 37 °C in 25 mM Tris–HCl (pH 7.5), and an aliquot removed when thioflavin T fluorescence reached ~5% of its final value; substrate, mica; final protein concentration in AFM, 0.1 μM. The height bar represents 15 nm. E, Cross-section of image D. F, Time series of 1.4 μm × 1.4 μm AFM height images. At 50 °C; buffer, 20 mM sodiumphosphate (pH 7.0), 1.3 mM putrescine, supplemented with 0.063 μM pre-aggregated α-synuclein wt; substrate, mica; monomeric protein concentration, 8 μM α-synuclein wt. The height bar represents 20 nm. G, Time-dependence of the fibril length of the four individual fibrils marked by color in the 32.0 min image in F. Note that double tip artifacts caused by protein adsorption to the tip are present in images A and C. Reported times indicate the time elapsed since monomer injection.

directionality and growth rates of amyloid fibrils has been observed.[38]

We can propose two factors accounting for the sparseness of the protofibril growth events. First, interaction of the spheroids with the substrate might perturb their potential for further assembly. Second, the spheroids might constitute intrinsically stable intermediates in the aggregation pathway. In fact, spheroids are found in intermediate fractions of α-synuclein incubated outside the AFM in addition to mature α-synuclein fibrils (Figure 5D and E). Spherical oligomers of somewhat smaller height (2–6 nm) were observed before in α-synuclein incubations.[25,27,29]

Whereas protofibril growth could be imaged by *in situ* AFM, growth of the mature fibrils was not observed. *In situ* AFM experiments were repeated in the presence of low concentrations of fibrillar α-synuclein aggregates preformed outside of the AFM. After acquiring images of these seeding structures, monomeric α-synuclein was added and fibril formation was monitored continuously. Mature fibrils did not grow further during the time of the experiment, although the growth of fibrils distinctly smaller than mature fibrils was observed. Figure 5F shows a time-course of α-synuclein wild-type self-assembly on a mica substrate in 20 mM sodium phosphate (pH 7.0) at protein concentrations of 8 μM for the injected monomeric protein and 0.06 μM for the pre-aggregated fibrillar protein in the presence of 1.3 mM putrescine at 50 °C. Recruitment of monomeric α-synuclein into the preformed structures, resulting in their elongation, was the predominant assembly mechanism, emphasizing the potential of these structures to seed fibril growth. The preformed structure consisted of a few adjoined fibrillar elements and exhibited a variable height in the range of 5–12 nm, suggesting that it represented a conglomerate of protofibrils possibly originating

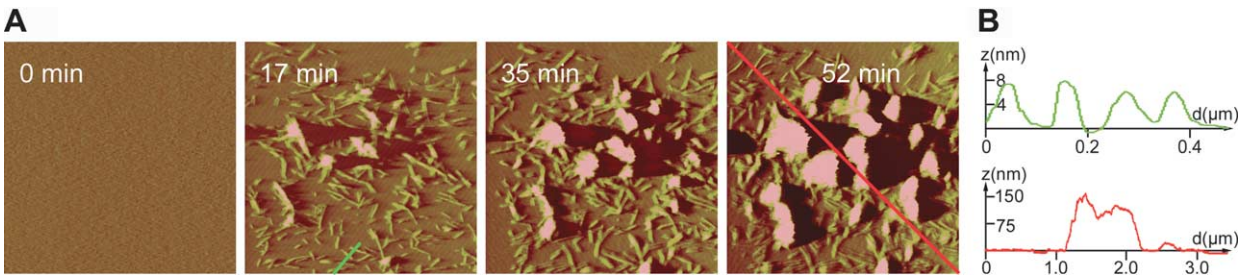

Figure 6. Fibrillar and amorphous aggregation at pH 5.0. A, Time series of 2.5 μm × 2.5 μm AFM amplitude images. The experiment was performed at 45 °C in 50 mM Na–Mes (pH 5.0), supplemented with 0.1 mM $MgCl_2$ utilizing a mica substrate. At $t = 0$ monomeric wild-type α-synuclein was added to a final concentration of 5 μM. B, Cross-sections of the AFM height images corresponding to the 17 minute (green) and 52 minute (red) amplitude images from A.

from a dissected mature fibril. The heights of the growing fibrils were typical for protofibrils (~5 nm), demonstrating once again that, in contrast to mature fibril growth, protofibril growth was observable by *in situ* AFM. Interestingly, according to the time dependence of fibril length, elongation did not proceed continuously but rather *via* a stop-and-run mechanism, as is evident from the plateaus observed temporarily for each of the protofibrils in Figure 5G. The average fibril growth rate was in the order of 10 nm/minute. However, due to the stepwise progression of fibrillation the maximum growth rate for a fibril observed between two images was ~50 nm/minute, a value significantly greater than the average rate. This value represented a lower limit for the maximum growth rate, inasmuch as the time required for the corresponding growth step might have been below the temporal resolution of the *in situ* AFM instrument (2.1 minutes per image).

Fibrils are formed initially at low pH and lead to amorphous aggregates

Incubating α-synuclein *in vitro* at low pH leads to accelerated aggregation with the formation of amorphous rather than fibrillar aggregates.[21,24] The latter retain certain features of amyloid structures, e.g. the ability to bind the fluorescent dye thioflavin T. We performed *in situ* AFM experiments at pH 5.0 and 45 °C (in the absence of polyamines) in order to follow continuously the formation of these aggregates. During the course of aggregation, fibrils constituted a distinct intermediate stage (Figure 6A). After rapid formation in the first few minutes, further fibril growth virtually ceased. Instead, deposition of amorphous material on the fibril surface became the primary mode of α-synuclein assembly, eventually leading to large amorphous aggregates with a height (up to 150 nm; Figure 6B) exceeding greatly that of the individual fibrils (~6–8 nm). We propose that the acidic C terminus is partially neutralized upon pH reduction, such that electrostatic repulsion between fibrils is reduced and both monomeric and multimeric α-synuclein are able to make favorable interactions with the fibril surface. The presence of both fibrillar and amorphous aggregates at pH 5.0 is consistent with experiments performed outside of the AFM.[21]

Discussion

The data presented here demonstrate the applicability of *in situ* tapping mode AFM for observation of α-synuclein self-assembly. The method offers important advantages. First, it allows continuous monitoring of individual aggregate species. Second, as is recapitulated in Figure 7, it is capable of providing high-resolution images of pre-fibrillar spheroid aggregates as well as the elongated sheet structures with heights consistent with that of a single β-sheet. Third, imaging in fluid offers the opportunity to apply various solution conditions, a crucial advantage considering the strong solution dependence of α-synuclein aggregation. The AFM setup employed in this work additionally permits the adjustment of the sample temperature, an essential feature given the influence of temperature on amyloid formation. A prerequisite for imaging of an object by AFM is its adhesion to the substrate surface. The selected substrate might bias the assembly process,[32] but this effect can be assessed by utilizing substrates of different chemical nature. In fact, several observations point towards a role of surface characteristics in α-synuclein aggregation and amyloid formation in general, both *in vitro* and *in vivo*.[39] α-Synuclein associates with membrane surfaces,[40,41] which leads to modulated aggregation properties.[42–45] The same holds true for anionic micelle surfaces.[46] The presence of a surface in *in situ* AFM therefore offers the opportunity to investigate the surface dependence of α-synuclein assembly even to the point of mimicking conditions similar to those *in vivo*.

Surface-templated formation of sheets with heights consistent with single β-sheets

Formation of 1.1(±0.2) nm high sheets was the

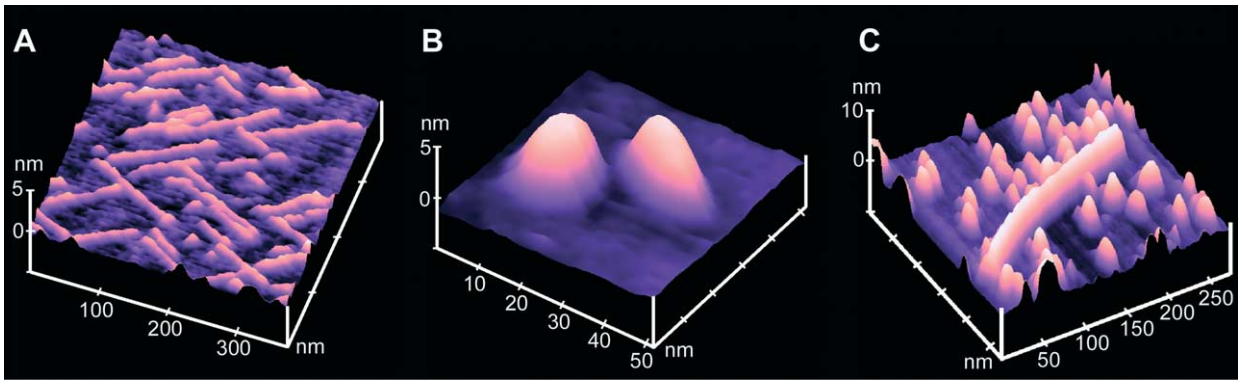

Figure 7. Surface view of the main aggregate morphologies observed in this study. A, Sheets; B, spheroids; C, protofibril and spheroids. A, The area displayed corresponds to a section of Figure 4A. B, Experimental conditions as for Figure 4B. C, The area displayed corresponds approximately to Figure 5A.

major self-assembly mode on mica substrates in the absence of the polyamines spermidine and spermine. The mica surface served as a template in this assembly process, as indicated by the following three observations. First, sheets grew in length on the surface, but elongated sheets did not appear spontaneously from solution. Second, sheet formation was dependent on the nature of the substrate and did not occur on hydrophobic HOPG in contrast to hydrophilic mica. Third, the sheets aligned along two specific directions that were separated by an angle of 120(±2)°, reflecting the pseudo-hexagonal surface geometry of mica (001). Interestingly, only two of the three directions expected for a perfect pseudo-hexagonal surface geometry governed the sheet directions. A similar phenomenon was reported for epitaxial growth of para-sexiphenyl thin films on mica and explained on the basis of the crystal structure of mica.[47] After cleavage in the (001) plane, the uppermost oxygen layer exhibits a pseudo-hexagonal geometry, while hydroxide and fluoride anions reside in the octahedral layer below. These anions are slightly dislocated from the center of the hexagonal openings of the top layer, resulting in a twofold symmetry of mica (001) surfaces.[35,47] The observation of two instead of three preferred directions for sheet formation thus indicates that this assembly process is influenced by the precise location of negative charges in the octahedral layer below the top oxygen layer.

The height of the sheet-like aggregates of 1.1(±0.2) nm was in the range expected for a single β-sheet. X-ray diffraction studies of α-synuclein fibrils yield a spacing of 1.0–1.1 nm between the β-sheets comprising the fibril.[12] The coinciding dimensions of the β-sheets constituting the fibrils and the sheets observed by *in situ* AFM suggest that the structures assembled on mica might constitute individual, elongated β-sheets, possibly sharing details of structural organization with those incorporated in the fibrils. The growth of β-sheet assemblies is likely to proceed by continuous binding of monomers to the β-strand located at the sheet end *via* hydrogen bonds. In this manner, the hydrogen bond network is extended and highly organized, and stable structures as typified by amyloid fibrils are formed.[31,48] Such an assembly mode requires that the hydrogen-bonding interface of the β-strand located at the sheet end points into the direction of sheet growth. Consequently, the individual β-strands constituting the sheet structures have to be oriented perpendicular to the long sheet axis, forming a cross-β-structure in analogy to the organization of β-sheets encountered in amyloid fibrils. Similar conclusions were drawn from *in situ* AFM studies of a different amyloidogenic peptide, Alzheimer's β-amyloid peptide (Aβ).[33] Aβ forms elongated sheet structures with heights of 1.0–1.2 nm, also exhibiting a distinct directionality of sheet alignment that reflects the lattice structure of the substrate. Likewise, elastin peptides that are known to assemble into aggregates rich in β-structure were reported to form substrate–lattice-oriented, sheet-like structures with a height of ~1.2 nm and a deconvolved width of ~3 nm in *in situ* AFM experiments.[49]

Importantly, the substrate required for sheet formation from α-synuclein was different from the one required for Aβ and elastin peptide sheet assembly. Aβ and elastin peptides form sheets on HOPG, but not on mica. The opposite is true for α-synuclein, showing that substrate-directed formation of β-sheets does not occur exclusively on hydrophobic surfaces. Amyloidogenic peptides and proteins thus appear to have a tendency to assemble on surfaces into single β-sheets, testifying to their potential to adopt β-structures, yet with different individual preferences for surfaces of different chemical nature. The surface properties required for β-sheet formation by a specific protein will consequently depend on its primary structure. Preferential assembly of α-synuclein on a negatively charged substrate such as mica is in accordance with previous observations of accelerated fibrillation in the presence of anionic micelle surfaces[46] and polyanions such as glycosaminoglycans[50] and DNA (D.C., W.H., V.S. & T.M.J., unpublished results). Interestingly, α-synuclein

itself is an acidic protein with a noticeable excess of negative charges at neutral pH. However, the acidic residues are concentrated in the C terminus (mainly residues 104–140) with the remainder of the protein exhibiting a positive net charge at neutral pH. In this context the comparison of sheet formation of full-length with C-terminally truncated α-synuclein is informative, suggesting that the C terminus is not incorporated into the sheet assemblies, analogous to the situation in mature fibrils,[14,15,36] but remains in solution. In this scenario, the positively charged N-terminal and central regions of the protein monomer can associate with the negatively charged substrate, whereas the C-terminal region does not interact with the surface. Possible mediators of favorable protein–surface interactions are the five KXK motifs present in the N-terminal part of the α-synuclein sequence. In a β-sheet conformation, two positively charged lysine residues would be located adjacently, facing in the same direction. Interestingly, model peptides with alternating hydrophobic and hydrophilic amino acids containing KXK motives were shown to assemble on mica, yielding nanofibers of similar morphology as reported here for α-synuclein.[51] Moreover, porphyrin self-assembles on mica in the presence of polylysine into rod-like structures that exhibit the same directionality observed for α-synuclein sheets,[52] providing further evidence for a potential role of lysine residues in substrate-governed peptide and protein self-assembly.

While sheet formation from wild-type α-synuclein and the A30P mutant were indistinguishable, A53T assembly occurred faster and the final structures appeared to be less organized. Similarly, in the presence of spermidine and spermine, A53T formed fewer spheroids compared to wild-type and A30P α-synuclein, but precipitated rapidly on the mica surface. These observations are compatible with previous studies reporting altered aggregation behavior, i.e. faster aggregation, as a consequence of the A53T mutation, which could account for its pathogenic effect.[12,25–28] The present study adds a further perspective to this issue in that it indicates that surface-directed aggregation might be of importance for the increased toxicity of the A53T mutant.

Spheroids are formed rapidly when polyamines are bound to the C terminus and constitute intermediates on the pathway towards fibrillar aggregates

In the presence of the polyamines spermidine and spermine, α-synuclein readily assembled into spheroids with heights of approximately 6 nm. Spheroid formation seemed to be a surface-independent process. First, the dimensions of the individual spheroids did not change in time after their first appearance. Second, the chemical nature of the substrate did not alter spheroid formation. Third, they were also encountered in incubations performed outside of the AFM. We conclude that increasing numbers of spheroids on the substrate with time reflects their surface-independent formation in solution. However, it cannot be absolutely excluded that surfaces might generally, i.e. independent of their chemical nature, assist spheroid formation.

The ability to assemble into spheroid structures appears to be a common property of amyloidogenic proteins and peptides. Several such structures with dimensions similar to those given here for α-synuclein have been reported in the literature and are referred to in different ways, e.g. as micelles, diffusible non-fibrillar ligands, single unit aggregates or soluble oligomers. For α-synuclein itself, spherical assemblies of 2–6 nm height were observed.[13,25,27,29] Aβ forms oligomeric units with heights between 4 nm and 6 nm.[33,34,53–56] The prion protein Sup35 and the immunoglobin light chain SMA assemble into spherical oligomers exhibiting heights of 2–4 nm and ~5.5 nm, respectively.[39,57] Recently, evidence has accumulated that such pre-fibrillar assemblies and not amyloid fibrils account for most of the toxicity of amyloidogenic proteins and peptides.[7,8,53] Kayed *et al*.[8] prepared Aβ-covered gold particles (mean diameter ~5.3 nm) as molecular mimics for soluble oligomers and used them as antigens in antibody production.[8] The antibody obtained inhibits the *in vitro* toxicity of different amyloidogenic peptides and proteins, including α-synuclein. The mechanism by which soluble oligomers mediate their toxicity is unclear. Membrane permeabilization represents one potential candidate and was proposed as the toxic function of pre-fibrillar α-synuclein.[5,58] Considering the suggested key role of spheroid structures for amyloid toxicity, the identification of factors promoting their formation by techniques such as *in situ* AFM is highly informative. In the experiments described here, the polyamines spermidine and spermine promoted spheroid formation. The naturally occurring polyamines putrescine, spermidine and spermine have been shown to accelerate amyloid aggregation of α-synuclein and their binding site was identified as the C terminus (residues 109–140).[22,23] The binding constants were between 0.6 mM and 10 mM with stronger binding linked to the higher number of positive charges and length of the polyamine. Electrostatic interactions of the negatively charged aspartate and glutamate residues in the C terminus of α-synuclein with the positively charged amino groups of the polyamine represent the driving force of binding, resulting in neutralization of charges specifically in the region between residues 109 and 140. Spheroid formation required the presence of one of the stronger binding polyamines spermidine or spermine, which saturate the protein to ~60% and ~25%, respectively, under the conditions used here based on the binding constants obtained from NMR.[23] In contrast, 1 mM putrescine with only ~9% saturation was ineffective in spheroid formation. Importantly, spheroids

were not formed from the C-terminally truncated protein syn(1–108) lacking the polyamine-binding site. We conclude that with its C terminus electrostatically shielded by bound polyamines full-length α-synuclein cannot be regarded as functionally equivalent to a truncated molecule lacking the C terminus. Thus, polyamine binding to the C terminus promotes spheroid formation not only indirectly by releasing the inherent inhibition by the negatively charged C terminus, but also directly by a yet unknown mechanism. The bridging of protein monomers by the multivalent polyamines would be one plausible mechanism. Alternatively, spheroid formation might be enhanced as a consequence of structural effects of polyamine binding on protein regions remote from the binding site but crucial for self-assembly. Such secondary effects of polyamine binding were suggested by NMR intensity changes in the N terminus and central region upon polyamine binding.[23] Up to now, the sole effect of the C terminus on α-synuclein self-assembly has been ascribed to a deceleration of aggregation.[12,16,17] With regard to spheroid formation, the results presented here indicate that this inhibitory function can reverse into an aggregation-promoting function upon polyamine binding.

Apart from the identity of the polyamine employed in the *in situ* AFM experiments, further factors, namely polyamine concentration, protein concentration and temperature, affected spheroid formation. All of these factors are known to bias fibrillation and spheroid formation of α-synuclein,[22,24,37] suggesting that spheroids possibly constitute on-pathway intermediates in the process of fibrillation. This view is supported by the observation that the 6 nm spheroids can evolve into fibrillar structures of similar height. The spheroid-protofibril transition was also described for Aβ, Sup35 and the immunoglobin light chain SMA.[33,34,39,54,55,57] The observation of spheroids as intermediates in α-synuclein incubations outside of the AFM and the sparseness of protofibril growth from spheroids encountered in *in situ* AFM together suggest that the spheroid–protofibril transition might constitute a key step in the fibrillation process.

Another explanation for the stability of spheroids in *in situ* AFM could be that their interaction with the substrate inhibits further growth. The surface-governed formation of protein sheets clearly demonstrates that the substrate influences α-synuclein assembly. Moreover, the fibrils visualized by *in situ* AFM were distinctly thinner than the mature fibrils representing the major morphology observed in samples that were aggregated outside of the AFM. The same phenomenon was observed for amylin, Aβ and immunoglobin light chain SMA fibrillation on mica substrates,[32,34,39] demonstrating that the presence of the mica surface modulates the accessible fibril morphologies. Finally, interactions with the substrate might also account for the rather surprising observation of a stop-and-run mechanism for protofibril elongation. Direct observation of amyloid fibrillation from β2-microgobulin by total internal reflection fluorescence microscopy did not support such a mechanism, although the growth rates of individual fibrils varied.[59] In *in situ* AFM, heterogeneous interactions of the protofibril ends with the surface could result in variable activation barriers for further recruitment of pre-fibrillar α-synuclein from solution, giving rise to the observed stop-and run-phases.

Incorporation of α-synuclein fibrils into amorphous aggregates is governed by the charge state of the fibril surface

At pH 5.0, α-synuclein first assembled into fibrillar structures that were subsequently covered with protein precipitates of amorphous morphology. It should be noted that the amorphous aggregates formed at low pH differ from unspecific protein aggregates in that they apparently share structural properties with amyloid aggregates.[21] The detection of amorphous aggregates originating from α-synuclein fibril surfaces could be explained by a potential of these surfaces to act as nucleation sites in amorphous aggregation under certain charge conditions. Alternatively, the amorphous aggregates might form in solution and the initially formed fibril surfaces could constitute the substrate for their deposition that is preferred to the charged mica plane. In both cases, the modulated electrostatic properties of the fibril surfaces upon pH reduction are the likely cause for their increased tendency to interact rather unspecifically compared to neutral pH. At neutral pH, the α-synuclein C terminus is not incorporated into the fibril core but located on the fibril surface.[14,15,36] If the same was true at pH 5.0, the fibril surface would carry a distinctly decreased charge at pH 5.0 compared to neutral pH due to the neutralization of the numerous acidic C-terminal residues. Consequently, hydrophobic interactions with the fibril surface would be facilitated, potentially culminating in rather unspecific amorphous aggregation. Unspecific interactions of protein aggregates with cellular compounds other than the amyloidogenic protein itself are thought to be a critical step in the pathogenesis of protein misfolding diseases.[7]

The observation and analysis of the diverse assembly modes presented here highlight many features that are important for aggregation of α-synuclein. In relation to the neurotoxicity of amyloid proteins, the detection of spontaneous formation of 6 nm high spheroid structures dependent on the solution conditions is very informative. These structures resemble the formerly described soluble oligomers, which were suggested to be the major toxic species in amyloid diseases.[8] Our experiments show that the formation of these structures is strongly favored when polyamines are bound to the C terminus (residues 109–140).

Apart from spheroids, assembly of α-synuclein can yield 1.1 nm high protein sheets, possibly individual β-sheets with a cross-β conformation similar to that present in amyloid fibrils. Interestingly, these sheets are formed preferentially on mica in a surface-templated manner, pointing towards the capability of α-synuclein to self-assemble on negatively charged surfaces. In the cellular context such surfaces are represented by anionic membrane phospholipid surfaces, with which α-synuclein readily associates *in vitro*, resulting in modulated aggregation properties.[40–45] The experimental setup employed in this work can be used for further investigation of the sheet growth and spheroid formation processes with respect to the underlying mechanisms and the identification of potential assembly inhibitors.

Materials and Methods

Preparation of wild-type, mutant and truncated α-synuclein

Recombinant human wild-type, A53T and A30P α-synuclein were expressed and purified as described[21] using plasmid pT7-7 encoding for the proteins (courtesy of the Lansbury laboratory, Harvard Medical School, Cambridge, MA). The carboxy-terminally truncated α-synuclein fragment syn(1–108) was amplified by PCR from full-length wild-type α-synuclein and subcloned into pT7-7. The sequence was validated by DNA sequencing. Expression and purification of the truncated proteins was performed essentially as described for full-length α-synuclein.[21] The identity of all proteins was verified by electrospray ionization mass spectrometry (ESI-MS). Protein concentrations were obtained using the bicinchoninic acid (BCA) assay and validated by absorbance measurements at 275 nm using an extinction coefficient of 1400 M^{-1} cm^{-1} per tyrosine residue.

Atomic force microscopy

AFM images were acquired on a Digital Instruments Multimode Nanoscope IIIa scanning probe microscope using an E-Scanner (Digital Instruments, Santa Barbara, CA). The scanner was equipped with a custom-built temperature controller comprising two tandem Peltier elements controlling the temperature of the sample and the scanner, respectively. This setup allowed for setting accurately defined elevated sample temperatures, while maintaining the scanner under constant thermal conditions. Freshly cleaved mica or HOPG were used as substrates for each experiment. The respective buffer supplemented with the desired concentration of polyamine and aliquots from solutions of preformed aggregates, when required, was deposited on the substrate in a total volume of either 80 μl or 90 μl. Polyamine stock solutions were prepared by diluting the respective chloride salts in water. The pH effect of polyamine addition to the *in situ* AFM solutions was <0.05 pH unit. For pH 5.0 experiments, $MgCl_2$ was added at a final concentration of 0.1 mM. The sample temperature controller was set to the desired temperature (33 °C, 45 °C or 50 °C) and kept constant during the experiment. The fluid cell was not sealed with an O-ring. The volume of liquid was kept constant by replacing evaporated water *via* a syringe, thus ensuring that the position of the meniscus did not change. After acquiring an initial image of the clean mica or HOPG surface (or a surface region comprising preformed aggregates, respectively), either 10 μl or 20 μl of monomeric α-synuclein in the same buffer as that added previously to the fluid cell were added *via* a syringe to yield a final volume of 100 μl and final concentrations as indicated in the text and Figure legends.

AFM images were acquired continuously at a scan rate between 1.00 Hz and 2.96 Hz with 256 lines per image, i.e. data acquisition took between 1.44 minutes and 4.27 minutes per image. Imaging was performed in tapping mode with either NP-S (Digital Instruments; nominal spring constant 0.32 N/m) or OMCL-TR800PSA (Olympus; nominal spring constant 0.57 N/m) cantilevers at an oscillation frequency of ~9 kHz.

In general, the indicated times refer to the moment when data acquisition for the respective image was completed. In contrast, time data in Figure 5G correspond to the time imaging of the particular fibril was accomplished.

Formation of preformed aggregates

Fibrillar α-synuclein aggregates were obtained by incubating 100 μM (Figure 5D and E) or 250 μM (preformed structures in Figure 5F and G) solutions of α-synuclein at 37 °C in glass vials under constant stirring with micro stir bars. The fibrillation process was followed by thioflavin T binding as described elsewhere[21] and stopped after a constant thioflavin T fluorescence intensity indicated that a steady-state was reached.

Acknowledgments

We thank Helmut Richmann for the construction of the tandem Peltier temperature controller. We are indebted to Herming Urlaub for the ESI-MS measurements. W.H. acknowledges support from the Stiftung Stipendien-Fonds des Verbandes der Chemischen Industrie and the Bundesministerium für Bildung und Forschung.

References

1. Goedert, M. (2001). Alpha-synuclein and neurodegenerative diseases. *Nature Rev. Neurosci.* **2**, 492–501.
2. Goldberg, M. S. & Lansbury, P. T., Jr (2000). Is there a cause-and-effect relationship between α-synuclein fibrillization and Parkinson's disease? *Nature Cell. Biol.* **2**, E115–E119.
3. Polymeropoulos, M. H., Lavedan, C., Leroy, E., Ide, S. E., Dehejia, A., Dutra, A. *et al.* (1997). Mutation in the α-synuclein gene identified in families with Parkinson's disease. *Science*, **276**, 2045–2047.
4. Kruger, R., Kuhn, W., Muller, T., Woitalla, D., Graeber, M., Kosel, S. *et al.* (1998). Ala30Pro mutation in the gene encoding α-synuclein in Parkinson's disease. *Nature Genet.* **18**, 106–108.
5. Lashuel, H. A., Hartley, D., Petre, B. M., Walz, T. & Lansbury, P. T., Jr (2002). Amyloid pores from pathogenic mutations. *Nature*, **418**, 291.

6. Kim, Y. S., Lee, D., Lee, E. K., Sung, J. Y., Chung, K. C., Kim, J. & Paik, S. R. (2001). Multiple ligand interaction of α-synuclein produced various forms of protein aggregates in the presence of Aβ25-35, copper, and eosin. *Brain Res.* **908**, 93–98.
7. Bucciantini, M., Giannoni, E., Chiti, F., Baroni, F., Formigli, L., Zurdo, J. *et al.* (2002). Inherent toxicity of aggregates implies a common mechanism for protein misfolding diseases. *Nature*, **416**, 507–511.
8. Kayed, R., Head, E., Thompson, J. L., McIntire, T. M., Milton, S. C., Cotman, C. W. & Glabe, C. G. (2003). Common structure of soluble amyloid oligomers implies common mechanism of pathogenesis. *Science*, **300**, 486–489.
9. Weinreb, P. H., Zhen, W., Poon, A. W., Conway, K. A. & Lansbury, P. T., Jr (1996). NACP, a protein implicated in Alzheimer's disease and learning, is natively unfolded. *Biochemistry*, **35**, 13709–13715.
10. Hashimoto, M., Hsu, L. J., Sisk, A., Xia, Y., Takeda, A., Sundsmo, M. & Masliah, E. (1998). Human recombinant NACP/α-synuclein is aggregated and fibrillated *in vitro*: relevance for Lewy body disease. *Brain Res.* **799**, 301–306.
11. Giasson, B. I., Uryu, K., Trojanowski, J. Q. & Lee, V. M. (1999). Mutant and wild type human α-synucleins assemble into elongated filaments with distinct morphologies *in vitro*. *J. Biol. Chem.* **274**, 7619–7622.
12. Serpell, L. C., Berriman, J., Jakes, R., Goedert, M. & Crowther, R. A. (2000). Fiber diffraction of synthetic α-synuclein filaments shows amyloid-like cross-β conformation. *Proc. Natl Acad. Sci. USA*, **97**, 4897–4902.
13. Conway, K. A., Harper, J. D. & Lansbury, P. T., Jr (2000). Fibrils formed *in vitro* from α-synuclein and two mutant forms linked to Parkinson's disease are typical amyloid. *Biochemistry*, **39**, 2552–2563.
14. Der-Sarkissian, A., Jao, C. C., Chen, J. & Langen, R. (2003). Structural organization of α-synuclein fibrils studied by site-directed spin labeling. *J. Biol. Chem.* **278**, 37530–37535.
15. Miake, H., Mizusawa, H., Iwatsubo, T. & Hasegawa, M. (2002). Biochemical characterization of the core structure of α-synuclein filaments. *J. Biol. Chem.* **277**, 19213–19219.
16. Crowther, R. A., Jakes, R., Spillantini, M. G. & Goedert, M. (1998). Synthetic filaments assembled from C-terminally truncated α-synuclein. *FEBS Letters*, **436**, 309–312.
17. Murray, I. V., Giasson, B. I., Quinn, S. M., Koppaka, V., Axelsen, P. H., Ischiropoulos, H. *et al.* (2003). Role of α-synuclein carboxy-terminus on fibril formation *in vitro*. *Biochemistry*, **42**, 8530–8540.
18. Paik, S. R., Shin, H. J., Lee, J. H., Chang, C. S. & Kim, J. (1999). Copper(II)-induced self-oligomerization of α-synuclein. *Biochem. J.* **340**, 821–828.
19. Nielsen, M. S., Vorum, H., Lindersson, E. & Jensen, P. H. (2001). Ca^{2+} binding to α-synuclein regulates ligand binding and oligomerization. *J. Biol. Chem.* **276**, 22680–22684.
20. Uversky, V. N., Li, J. & Fink, A. L. (2001). Metal-triggered structural transformations, aggregation, and fibrillation of human α-synuclein. A possible molecular link between Parkinson's disease and heavy metal exposure. *J. Biol. Chem.* **276**, 44284–44296.
21. Hoyer, W., Antony, T., Cherny, D., Heim, G., Jovin, T. M. & Subramaniam, V. (2002). Dependence of α-synuclein aggregate morphology on solution conditions. *J. Mol. Biol.* **322**, 383–393.
22. Antony, T., Hoyer, W., Cherny, D., Heim, G., Jovin, T. M. & Subramaniam, V. (2003). Cellular polyamines promote the aggregation of α-synuclein. *J. Biol. Chem.* **278**, 3235–3240.
23. Fernandez, C. O., Hoyer, W., Zweckstetter, M., Jares-Erijman, E. A., Subramaniam, V., Griesinger, C. & Jovin, T. M. (2004). NMR of α-synuclein complexes with polyamines elucidates the mechanism and kinetics of induced aggregation. *EMBO J.* **23**, 2039–2046.
24. Uversky, V. N., Li, J. & Fink, A. L. (2001). Evidence for a partially folded intermediate in α-synuclein fibril formation. *J. Biol. Chem.* **276**, 10737–10744.
25. Conway, K. A., Harper, J. D. & Lansbury, P. T., Jr (1998). Jr accelerated *in vitro* fibril formation by a mutant α-synuclein linked to early-onset Parkinson's disease. *Nature Med.* **4**, 1318–1320.
26. Narhi, L., Wood, S. J., Steavenson, S., Jiang, Y., Wu, G. M., Anafi, D. *et al.* (1999). Both familial Parkinson's disease mutations accelerate α-synuclein aggregation. *J. Biol. Chem.* **274**, 9843–9846.
27. Conway, K. A., Lee, S. J., Rochet, J. C., Ding, T. T., Williamson, R. E. & Lansbury, P. T., Jr (2000). Acceleration of oligomerization, not fibrillization, is a shared property of both α-synuclein mutations linked to early-onset Parkinson's disease: implications for pathogenesis and therapy. *Proc. Natl Acad. Sci. USA*, **97**, 571–576.
28. Li, J., Uversky, V. N. & Fink, A. L. (2001). Effect of familial Parkinson's disease point mutations A30P and A53T on the structural properties, aggregation, and fibrillation of human α-synuclein. *Biochemistry*, **40**, 11604–11613.
29. Ding, T. T., Lee, S. J., Rochet, J. C. & Lansbury, P. T., Jr (2002). Annular α-synuclein protofibrils are produced when spherical protofibrils are incubated in solution or bound to brain-derived membranes. *Biochemistry*, **41**, 10209–10217.
30. Lashuel, H. A., Petre, B. M., Wall, J., Simon, M., Nowak, R. J., Walz, T. & Lansbury, P. T., Jr (2002). α-Synuclein, especially the Parkinson's disease-associated mutants, forms pore-like annular and tubular protofibrils. *J. Mol. Biol.* **322**, 1089–1102.
31. Dobson, C. M. (2003). Protein folding and misfolding. *Nature*, **426**, 884–890.
32. Goldsbury, C., Kistler, J., Aebi, U., Arvinte, T. & Cooper, G. J. (1999). Watching amyloid fibrils grow by time-lapse atomic force microscopy. *J. Mol. Biol.* **285**, 33–39.
33. Kowalewski, T. & Holtzman, D. M. (1999). *In situ* atomic force microscopy study of Alzheimer's β-amyloid peptide on different substrates: new insights into mechanism of β-sheet formation. *Proc. Natl Acad. Sci. USA*, **96**, 3688–3693.
34. Blackley, H. K., Sanders, G. H., Davies, M. C., Roberts, C. J., Tendler, S. J. & Wilkinson, M. J. (2000). *In-situ* atomic force microscopy study of β-amyloid fibrillization. *J. Mol. Biol.* **298**, 833–840.
35. Bailey, S. W. (1980). Structures of layer silicates. In *Crystal Structure of Clay Minerals and their X-ray Identification* (Brindley, G. W. & Brown, G., eds), pp. 2–196, Mineralogical Society, London.
36. Crowther, R. A., Daniel, S. E. & Goedert, M. (2000). Characterisation of isolated α-synuclein filaments from substantia nigra of Parkinson's disease brain. *Neurosci. Letters*, **292**, 128–130.
37. Wood, S. J., Wypych, J., Steavenson, S., Louis, J. C., Citron, M. & Biere, A. L. (1999). α-Synuclein fibrillogenesis is nucleation-dependent. Implications for

the pathogenesis of Parkinson's disease. *J. Biol. Chem.* **274**, 19509–19512.
38. DePace, A. H. & Weissman, J. S. (2002). Origins and kinetic consequences of diversity in Sup35 yeast prion fibers. *Nature Struct. Biol.* **9**, 389–396.
39. Zhu, M., Souillac, P. O., Ionescu-Zanetti, C., Carter, S. A. & Fink, A. L. (2002). Surface-catalyzed amyloid fibril formation. *J. Biol. Chem.* **277**, 50914–50922.
40. Davidson, W. S., Jonas, A., Clayton, D. F. & George, J. M. (1998). Stabilization of α-synuclein secondary structure upon binding to synthetic membranes. *J. Biol. Chem.* **273**, 9443–9449.
41. McLean, P. J., Kawamata, H., Ribich, S. & Hyman, B. T. (2000). Membrane association and protein conformation of α-synuclein in intact neurons. Effect of Parkinson's disease-linked mutations. *J. Biol. Chem.* **275**, 8812–8816.
42. Jo, E., McLaurin, J., Yip, C. M., St George-Hyslop, P. & Fraser, P. E. (2000). α-Synuclein membrane interactions and lipid specificity. *J. Biol. Chem.* **275**, 34328–34334.
43. Lee, H. J., Choi, C. & Lee, S. J. (2002). Membrane-bound α-synuclein has a high aggregation propensity and the ability to seed the aggregation of the cytosolic form. *J. Biol. Chem.* **277**, 671–678.
44. Narayanan, V. & Scarlata, S. (2001). Membrane binding and self-association of α-synucleins. *Biochemistry*, **40**, 9927–9934.
45. Zhu, M. & Fink, A. L. (2003). Lipid binding inhibits α-synuclein fibril formation. *J. Biol. Chem.* **278**, 16873–16877.
46. Necula, M., Chirita, C. N. & Kuret, J. (2003). Rapid anionic micelle-mediated α-synuclein fibrillization *in vitro*. *J. Biol. Chem.* **278**, 46674–46680.
47. Plank, H., Resel, R., Andreev, A., Sariciftci, N. S. & Sitter, H. (2002). Structural relationship between epitaxially grown para-sexiphenyl and mica (0 0 1) substrates. *J. Cryst. Growth*, **237–239**, 2076–2081.
48. Jaroniec, C. P., MacPhee, C. E., Bajaj, V. S., McMahon, M. T., Dobson, C. M. & Griffin, R. G. (2004). High-resolution molecular structure of a peptide in an amyloid fibril determined by magic angle spinning NMR spectroscopy. *Proc. Natl Acad. Sci. USA*, **101**, 711–716.
49. Yang, G., Woodhouse, K. A. & Yip, C. M. (2002). Substrate-facilitated assembly of elastin-like peptides: studies by variable-temperature *in situ* atomic force microscopy. *J. Am. Chem. Soc.* **124**, 10648–10649.
50. Cohlberg, J. A., Li, J., Uversky, V. N. & Fink, A. L. (2002). Heparin and other glycosaminoglycans stimulate the formation of amyloid fibrils from α-synuclein *in vitro*. *Biochemistry*, **41**, 1502–1511.
51. Hong, Y., Legge, R. L., Zhang, S. & Chen, P. (2003). Effect of amino acid sequence and pH on nanofiber formation of self-assembling peptides EAK16-II and EAK16-IV. *Biomacromolecules*, **4**, 1433–1442.
52. Koti, A. S. R. & Periasamy, N. (2003). Self-assembly of template-directed J-aggregates of porphyrin. *Chem. Mater.* **15**, 369–371.
53. Lambert, M. P., Barlow, A. K., Chromy, B. A., Edwards, C., Freed, R., Liosatos, M. *et al.* (1998). Diffusible, nonfibrillar ligands derived from Aβ1-42 are potent central nervous system neurotoxins. *Proc. Natl Acad. Sci. USA*, **95**, 6448–6453.
54. Nybo, M., Svehag, S. E. & Holm Nielsen, E. (1999). An ultrastructural study of amyloid intermediates in $A\beta_{1\text{-}42}$ fibrillogenesis. *Scand. J. Immunol.* **49**, 219–223.
55. Harper, J. D., Wong, S. S., Lieber, C. M. & Lansbury, P. T., Jr (1999). Assembly of Aβ amyloid protofibrils: an *in vitro* model for a possible early event in Alzheimer's disease. *Biochemistry*, **38**, 8972–8980.
56. Yong, W., Lomakin, A., Kirkitadze, M. D., Teplow, D. B., Chen, S. H. & Benedek, G. B. (2002). Structure determination of micelle-like intermediates in amyloid β-protein fibril assembly by using small angle neutron scattering. *Proc. Natl Acad. Sci. USA*, **99**, 150–154.
57. Serio, T. R., Cashikar, A. G., Kowal, A. S., Sawicki, G. J., Moslehi, J. J., Serpell, L. *et al.* (2000). Nucleated conformational conversion and the replication of conformational information by a prion determinant. *Science*, **289**, 1317–1321.
58. Volles, M. J., Lee, S. J., Rochet, J. C., Shtilerman, M. D., Ding, T. T., Kessler, J. C. & Lansbury, P. T., Jr (2001). Vesicle permeabilization by protofibrillar α-synuclein: implications for the pathogenesis and treatment of Parkinson's disease. *Biochemistry*, **40**, 7812–7819.
59. Ban, T., Hamada, D., Hasegawa, K., Naiki, H. & Goto, Y. (2003). Direct observation of amyloid fibril growth monitored by Thioflavin T fluorescence. *J. Biol. Chem.* **278**, 16462–16465.
60. Zarrane, J. J., Alegre, J., Gomez-Esteban, J. C., Lezcano, E., Ros, R., Ampyero, I. *et al.* (2004). The new mutation E46K of α-synuclein causes Parkinson and Lewy body dementia. *Ann. Neurol.* **55**, 164–173.

Edited by M. Yaniv

(Received 9 February 2004; accepted 9 April 2004)